Electronic band structure and luminescence properties of powdered ZrP_2O_7 crystals

Nedilko S. and Chornii V.

Taras Shevchenko National University of Kyiv, 64/13 Volodymyrska Street, 01601 Kyiv, Ukraine

Received: 13.08.2013

Abstract. Ultraviolet and visible photoluminescence properties of ZrP_2O_7 crystals are studied under excitation in the region 3.5÷12 eV of incident photon energies. Partial densities of electronic states are calculated with a full-potential linear augmented plane-wave method for both perfect crystals and those containing two types of oxygen vacancies. The UV luminescence is considered as a radiation decay of trapped excitons formed on the basis of $[ZrO_6]^{8-}$ polyhedrons. Generation of the excitons is mainly related to charge-transfer electronic transitions between the electronic states O*p* and Zr*d*. The visible luminescence and its excitation are associated with processes that occur in polyhedrons containing the oxygen vacancies.

Keywords: electronic band structure, visible luminescence, vacancy state

PACS: 71.20 -b, 78.55.Hx
UDC: 535.37

1. Introduction

Recently it has been found that ZrP_2O_7 crystals are promising for various applications as a material for mercury-free lamps and plasma display panels [1, 2]. Both pure Zr-containing materials and those doped with rare-earth ions represent well known X-ray phosphors with intense luminescence in ultraviolet (UV) and visible spectral regions [3, 4]. This practical aspect has stipulated a great number of researches dealing with luminescence of Zr-containing phosphates stimulated mainly with the band-to-band excitation [1–4]. As a result, the origin of luminescence centres in these materials has been described for a strong UV emission band with the maximum located near 300 nm (~ 4.1 eV). It is known that this emission corresponds to charge-transfer processes in ZrO_6 octahedra [1, 3, 5].

Recently the authors of the study [5] have shown that ZrP_2O_7 crystals are capable to luminesce in the visible optical region, too. It is obvious that the visible luminescence could decrease the intensity of the main UV band. Therefore understanding of nature of the visible luminescence is important while managing the UV-emission efficiency of ZrP_2O_7. As a consequence, the main purposes of this work are clarifying the nature of the visible luminescence in ZrP_2O_7 crystals and revealing its possible relationships with the UV-luminescence mechanisms. In order to reach this goal, we combine the results of experimental luminescent spectroscopy and theoretical calculations. It is known that the visible luminescence in undoped oxide materials is usually caused by uncontrolled impurities [6] or defect-related centres (e.g., F, F^+ or F_2^+ centres) [7–9]. Here we study the impact of oxygen vacancies on the luminescence properties of ZrP_2O_7 crystals. We are to notice that partial densities of states (PDOS) for ZrP_2O_7 with the oxygen vacancies have been calculated for the first time and so we hope that the data presented in the present work will be useful for understanding of luminescence properties of many other oxide solids.

2. Details of experiments and calculations

Powdered ZrP_2O_7 crystals were synthesized at the Inorganic Chemistry Department (Faculty of Chemistry, Taras Shevchenko National University of Kyiv, Ukraine). Crystalline ZrP_2O_7 was synthesized by crystallization of $LiPO_3$ melt containing 1.5 wt. % of ZrO_2 (for more details see Ref. [5]).

Luminescence spectroscopy experiments under excitation by a VUV synchrotron radiation were carried out at the SUPERLUMI station (HASYLAB (DESY), Hamburg, Germany) [10]. The photoluminescence (PL) spectra were obtained for the excitation energy region 3.5÷12 eV at the temperatures T = 8 K and 300 K. A N_2 laser (the radiation wavelength of λ_{ex} = 337.1 nm) was used as an additional source for exciting the PL in the UV region. All the measured PL emission and excitation spectra were corrected by a system response.

Electronic structures of ZrP_2O_7 with the oxygen vacancies and the corresponding perfect crystals were calculated using a WIEN2k program package (version 11.1) [11], in which a full-potential linear-augmented plane-wave technique was implemented in the framework of density-functional theory. The crystalline structure of the ZrP_2O_7 compound was taken from the literature (see Ref. [12]). The convolutions of the densities of electronic states (CDOS) in ZrP_2O_7 crystal were performed for the bandgap value E_g = 6.4 eV.

3. Results and discussion

ZrO_6 polyhedrons in ZrP_2O_7 crystals are regular octahedra with six Zr–O distances equal to 1.97 Å [12] (see Fig. 1a). There are two different positions for oxygen atoms in the zirconium pyrophosphate and, therefore, two types of oxygen vacancies could be formed. The nearest surroundings of these two types of vacancies are shown in Fig. 1b and Fig. 1c. The first type of vacancy denoted hereafter as V_O corresponds to oxygen that connects anionic group $P_2O_7^{4-}$ with Zr^{4+} ion via an ionic-type bond. It is clearly seen from Fig. 1c that the vacancy of the second type (referred hereafter to as $V_O^{/}$) is a vacancy of 'bridge' oxygen in anionic molecular group $P_2O_7^{4-}$. Usually, the covalent bonds inside the molecular group are stronger than the ionic bonds between the cations and the anionic groups. So, it would be quite reasonable to assume that the probability of formation of the first-type oxygen vacancy is higher than that of the 'bridge' oxygen vacancy. Therefore, if the visible luminescence in ZrP_2O_7 is really associated with the oxygen vacancies, the corresponding luminescence centres should be mainly formed owing to the V_O defects.

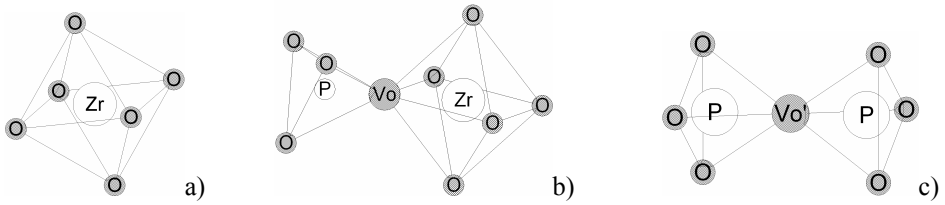

Fig. 1. Some details of ZrP_2O_7 crystal structure: (a) ZrO_6 octahedron; (b) nearest surrounding of the first-type oxygen vacancy V_O; (c) surrounding of the second-type oxygen vacancy $V_O^{/}$.

The PDOS calculated for the perfect ZrP_2O_7 crystals are presented in Fig. 2a. One can see that the valence band (VB) is formed mainly from O*p* states and zirconium states dominate at the bottom of the conduction band (CB). The PDOS of ZrP_2O_7:V_O crystals demonstrate some analogies with the PDOS calculated for the perfect zirconium pyrophosphate (see Fig. 2b). However, there are several essential differences between the perfect and defective crystals mentioned above. First of all, these are full-occupied vacancy states (FOVS) that arise near the middle of the forbidden band in ZrP_2O_7.

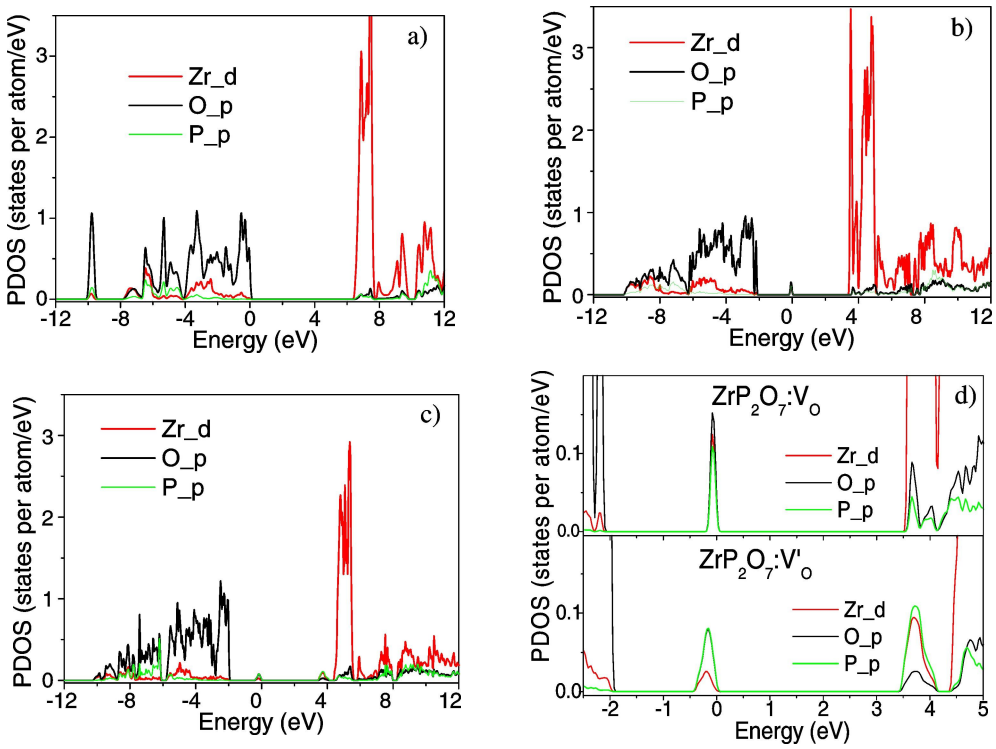

Fig. 2. PDOS for ZrP_2O_7 (a), ZrP_2O_7:V_O (b) and ZrP_2O_7:$V_O^{/}$ (c) crystals. Parts of panels (b) and (c) are shown in panel (d).

Similar situation has recently been observed for cubic ZrO_2 crystals with oxygen vacancies, where the vacancy states are formed by symmetric superposition of *d* orbital of four Zr^{4+} ions located nearest to the vacancy. In contrast to the cubic ZrO_2, the vacancy states in ZrP_2O_7:V_O crystals are formed by superposition of Zr*d*, O*p* and P*p* orbitals (see the top of Fig. 2d). Moreover, another higher-energy vacancy-related state (VRS) appears close to the bottom of the CB. This state is mainly formed by Zr*d* orbitals and its width is equal to ≈ 0.2 eV.

The VB and the CB in ZrP_2O_7:$V_O^{/}$ crystals are mainly formed by O2*p* and Zr4*d* orbitals, respectively (see Fig. 2c). Two VRS in the forbidden band are clearly observed (see Fig. 2d, bottom). Middle-gap vacancy state is fully occupied and it is nothing but a FOVS. In contrast to ZrP_2O_7:V_O, this state is mainly formed due to the orbitals of defective molecular anionic group [$P_2O_6 + V_O^{/}$]. A shallow acceptor level near the bottom of the CB, which represents a VRS, is formed by Zr*d* and P*p* orbitals. It has a low density of states, when compared with the similar level occurring in ZrP_2O_7:V_O.

Summarizing, the distances from the top VB to the FOVS and VRS levels are evaluated as being 1.7 eV (for the defect FOVS level $V_O^{/}$), 2.1 (for the defect FOVS level V_O), 5.3 (for the defect RVS level $V_O^{/}$), and 5.9 eV (for the defect RVS level V_O). According to these distances, we can assume a possible impact of non-radiative thermo-stimulated electron transitions from the VRS levels to the CB in ZrP_2O_7 crystals. In particular, this effect can be significant for the ZrP_2O_7 crystals containing the V_O defects, as here the VRS is located 0.5 eV lower with respect to the bottom of the CB. Below we will discuss a role of the FOVS and VRS levels in excitation of the PL in a more detail.

Taking into account the E_g value and the results of our calculations, we have measured the PL spectra under excitation of the next three types (see Fig. 3): at the band-to-band transitions

($hv_{ex} > E_g = 6.4$ eV), near the absorption edge ($hv_{ex} \approx E_g$), and inside the forbidden band of the pure crystals ($hv_{ex} < E_g$).

Only one UV emission band with the peak position $hv_{lum}^{max} = 4.13$ eV is observed at various band-to-band excitation transitions ($hv_{ex} = 6.7$ eV – see, e.g., curve 1 in Fig. 3). In case of excitation near the absorption edge ($hv_{ex} = 6.20$ eV – see curve 2 in Fig. 3), four additional bands of the visible PL arise at $hv_{lum}^{max} \approx 3.7$, 3.02, 2.50 and 2.10 eV, which are referred to as V1, V2, V3 and V4. These visible components of the PL spectra are strongly overlapped. So, the first of them, V1, is observed only as a tail of the UV luminescence band. The intensity of the visible PL is about 10 times smaller than that of the UV-band intensity. In case of excitation inside the forbidden band, the UV band vanishes and only a wide complex band of the visible PL is observed, with the peak positioned near 2.57 eV (see Fig. 3, curve 3).

The PL excitation spectra show an intense band with the maximum hv_{ex}^{max} located near 6.7 eV and two overlapping bands in the region 7.5÷10.5 eV, if the luminescence is monitored at the peak position of the UV band ($hv_{reg} = 4.13$ eV). The third excitation band is observed at the photon energies higher than 10.5 eV (see curve 1 in Fig. 4). When the temperature increases from 8 K up to the room one (300 K), the peak position of the main UV PL excitation band (6.7 eV) shifts towards lower-energy side (hv_{ex}^{max} at the room temperature being equal to 6.5 eV), while the full width at half height of the band increases (see Fig. 4, curve 2). In fact, the behaviour of the full width at half height for this band reveals increasing asymmetry on the high-energy side. A low-intensity band of the UV PL excitation can also be found in the region 5.5÷6.5 eV (see curve 1 in Fig. 4).

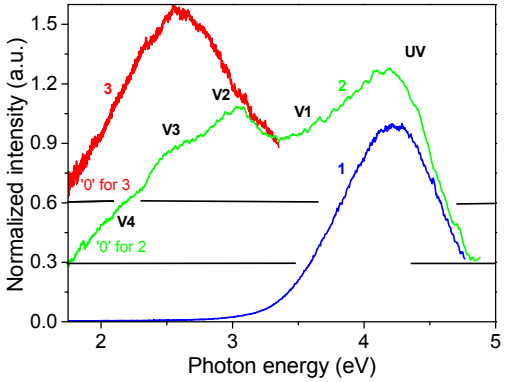

Fig. 3. PL spectra for ZrP_2O_7 crystals at $hv_{ex} = 6.70$ (curve 1), 6.20 (curve 2) and 3.68 eV (curve 3). The temperature is equal to $T = 8$ K.

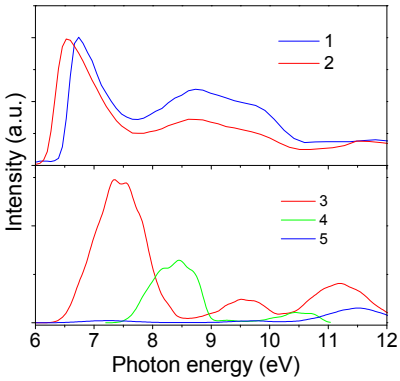

Fig. 4. PL excitation spectra for ZrP_2O_7 crystals at $hv_{reg} = 4.13$ (curves 1 and 2), and CDOS [O*p**Zrd] (curves 3 and 4) and [O*p**P*p*] (curve 5). The temperature is $T = 8$ (curve 1) and 300 K (curve 2). See details in the text.

To clarify the nature of the UV PL, we have compared some characteristics (e.g., the shapes and the band positions) of the PL excitation spectra with the calculated CDOS (see curves 3 to 5 in Fig. 4). A number of preliminary remarks should be done prior to discussion of the excitation processes peculiar for the PL emission. First, it is obvious that the CDOS should mainly correlate with the absorption spectra. However, in our case it is impossible to measure the absorption since the pyrophosphate crystals under test represent micro- and nanopowders. So, in this study we can only compare the CDOS and the PL excitation spectra. As for the excitation spectra, anti-

correlation between the excitation and the absorption spectra on the low-energy side of the fundamental absorption is usually observed for the materials with strong absorption [14]. This fact is due to strong absorption of exciting light and the following large losses of excitation energy on the crystal surface. This behaviour is especially typical for powdered micro- and nano-sized materials, where the role of surface is very important. ZrP_2O_7 samples investigated here are just the case. That is why the bandgap for calculating the CDOS has been chosen considering that the excitation spectra of the UV emission and the CDOS curves at the edge of the excitation spectra should anti-correlate, while a correlation has to take place for a higher-energy region of the excitation spectra. As a result, the E_g value obtained from our fitting is equal to 6.4 eV.

It is clear that the main excitation peak of the UV emission is located on the low-energy side of the calculated CDOS (see Fig. 4, curves 1 and 3). The CDOS curve 3 in Fig. 4 corresponds to the transitions from O*p* states of the top of the VB (–1.2÷0.0 eV) to Zr*d* states of the CB in the region 6.4÷11.7 eV (this convolution is marked as [O*p**Zr*d*]). The anti-correlation between curves 1 and 3 is observed in the energy region 6.7÷9.1 eV and the correlation between the experimental spectra and [O*p**Zr*d*] occurs for the energies higher than 9.1 eV. Good correlation with the excitation spectra is also observed for the CDOS obtained as convolution of the O*p* states in the deeper part of the VB (–1.8÷–1.2 eV) and the Zr*d* states in the energy region 6.4÷11.7 eV of the CB (see curve 4 in Fig. 4). The [O*p**P*p*]) CDOS for the O*p* states in the top of the VB (–1.2÷0.0 eV) and the P*p* states of the CB in the region 6.4÷11.7 eV are shown in Fig. 4 (see curve 5). Being associated with the transitions in oxide phosphate group, this CDOS has significant intensity, when compared with the $O \rightarrow Zr$ transitions, only at the energies higher than 10.5 eV. Thus, we conclude that the UV component of the PL is excited under the band-to-band transitions and the most efficient excitation takes place near the absorption edge.

It should be mentioned that the convolution curves do not reflect the shapes of the absorption and excitation spectra closely enough, as they do not account for transition probabilities. So, the real contributions of the two types of transitions, $O \rightarrow Zr$ and O*p* $\rightarrow$ P*p*, to the excitation spectra of the UV PL can differ from the relative intensities of the CDOS shown in Fig. 4 and Fig. 5 (see below). This especially concerns the [O*p**P*p*] curve. Indeed, it is common knowledge that the transitions within oxide molecular groups (i.e., phosphate groups in our case) give a considerable contribution to absorption of the dielectric oxide compounds in the energy region far from the absorption edge [1–3]. In any case, we suppose that the PL excitation with the photon energies $h\nu_{ex} < 10.5$ eV takes place within ZrO_6^{8-} polyhedrons.

Taking into consideration all the statements mentioned above, we can assume the following mechanism for the UV luminescence in ZrP_2O_7 crystals at low temperatures (4÷8 K). Direct excitation of ZrO_6^{8-} polyhedrons takes place at the excitation photon energies 6.4÷7.5 eV and this excitation reveals a character of the $O \rightarrow Zr$ charge transfer. Consequent changes in the electronic configuration of the polyhedrons cause deformations of ZrO_6 octahedron and therefore a molecular exciton $(ZrO_6^{8-})^*$ is formed in excited electron vibration state. This molecular exciton interacts with the lattice deformations and becomes self-trapped. Electronic component of the exciton is localized at the Zr^{4+} ion, $(Zr^{4+} + e^-) = (Zr^{3+})$, and its hole component is at the oxygen ion, $(O^{2-} - e^-) = (O^-)$. Radiation decay of such a self-trapped exciton is accompanied with the $Zr \rightarrow O$ charge-transfer process, thus causing strong UV luminescence. Absorption of the incident light in the region of 7.5÷10.5 eV generates electron-hole pairs. Recombination of those pairs at the ZrO_6^{8-} polyhedrons gives rise to excitons; then the excitons are localized and, finally, their radiation decay occurs in the manner similar to that described above.

In other words, the UV luminescence results mainly from the processes inside the spatial areas of perfect/regular crystal, though defective areas also play some part in generating the UV PL, if the temperature increases from 8 K to the room one. In fact, at low temperatures the VRS near the bottom of the CB mainly act as traps for electrons of the CB and so they quench the UV PL. When the temperature increases, the trapped electrons are released, thus causing increase in the UV luminescence intensity. At the same time, thermo-stimulated transitions for the electrons at the room temperature occur from the top of the VB to the VRS. As a result, a low-energy component of the UV-luminescence excitation in the spectral region of 6.0÷6.5 eV increases, manifesting itself as a shift of the excitation band (see curves 1 and 2 in Fig. 4).

Hence, the UV PL results from the processes in the regular spatial areas of our crystals, whereas the visible PL corresponds to defect-related luminescence occurring in the areas containing defects. Further evidences for this statement will be provided below.

In contrast to the UV emission, the most efficient excitation of the visible luminescence is observed at $hv_{ex} < E_g$ (see curve 1 in Fig. 5). Although this fact itself points to defect-related origin of the visible luminescence in ZrP_2O_7, the nature of the visible PL is not clear because it can be associated with both crystal lattice defects (e.g., oxygen vacancies, interstitial oxygen atoms, etc.) and non-controlled impurities (Zr-like ions such as Hf, Ti, etc.). Here we investigate only a possible role of oxygen vacancies in the visible luminescence of ZrP_2O_7.

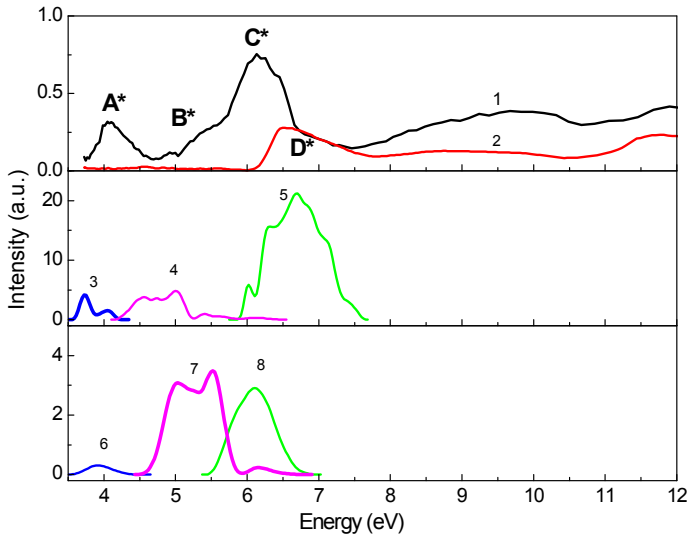

Fig. 5. PL excitation spectra for ZrP_2O_7 crystals at hv_{reg} = 2.76 (curve 1) and 3.02 eV (curve 2), and T = 300 (curve 1) and 8 K (curve 2); CDOS calculated for ZrP_2O_7:V_O (curves 3 to 5) and ZrP_2O_7: $V_O^{/}$ (curves 6 to 8) crystals. See details in the text.

If the luminescence is detected at the low temperature (8 K) in the visible range (hv_{reg} = 3.02 eV; the light wavelength 410 nm), the excitation spectrum is very similar to that observed for the UV PL at the room temperature (see Fig. 5, curve 2). One can see a main band D* at hv_{ex}^{max} = 6.5 eV, and several wide bands at higher energies. The additional small-intensity excitation bands are located at 4.0÷6.0 eV (see Fig. 5, curve 2). The intensity of the mentioned bands on the lower-energy side of the PL spectrum (hv_{reg} = 2.76 eV, i.e. ~ 450 nm) increases when the luminescence is detected at the room temperature; then a sharp excitation band A* is observed at hv_{ex}^{max} = 4.13 eV. At least, two components form this band (see Fig. 5, curve 1). The other excita-

tion band B* located in the region of 5÷6 eV also includes two details: a small-intensity band near 5.0 eV and a wide shoulder observed against the background of the main band. Finally, a band C* is located at 5.5÷7.0 eV, with a possible peak positioned near 6.1 eV (see Fig. 5, curve 1).

To reveal the origin of the bands in the visible PL excitation spectra, we have calculated several CDOS for the defective ZrP_2O_7:V_O and ZrP_2O_7:$V_O^{/}$ crystals (see Fig. 5, curves 3 to 8) and compared them with the experimental excitation spectra. Fig. 5 evidences that the CDOS labelled as 3 and 6 in Fig. 5 lie in the same spectral region as the A* band in the PL excitation spectra. The curves 3 and 6 correspond to convolutions of the FOVS and the VRS, [FOVS*VRS], for ZrP_2O_7:V_O and ZrP_2O_7:V_O' respectively. Let us notice that the bands corresponding to curve 3 are about one order of magnitude more intense than the bands related to the curve 6. Therefore it is most likely that the PL excited in the A* band is mainly linked with the V_O-type vacancies.

Another complex band seen in the excitation spectra, the B* band, coincides with superposition of the CDOS 4 and 7, which represent convolutions of the FOVS and Zr*d* states at the bottom of the CB (6.4÷8.5 eV); here curve 4 corresponds to ZrP_2O_7:V_O and curve 7 to ZrP_2O_7:$V_O^{/}$ crystals (see Fig. 5).

The CDOS curves 5 and 8 are convolutions of the O*p* states at the top of the VB (–3.6÷–2,3 eV for the V_O defects and –2.9÷–2,0 eV for the $V_O^{/}$ defects) and the VRS near the CB bottom for ZrP_2O_7:V_O and ZrP_2O_7:$V_O^{/}$ crystals, respectively. These curves coincide well with the excitation bands C* (curve 8) and D* (curve 5).

Together with the data on the positions of VRS summarized above, the interpretation of the excitation spectra provided here allows us to suppose the following mechanisms of the visible PL.

First, we are to notice similarity of the excitation spectra detected for $h\nu_{reg}$ = 3.02 eV (mainly for the PL bands V1 and V2) at T = 8 K, on the one hand, and the excitation spectra of the UV PL obtained at T = 300 K, on the other hand, when thermo-stimulated processes take place from the VRS level. Then, the low-energy component of the spectrum, the D* band, corresponds to the excitation channel 'the VB top $\rightarrow$ the VRS of V_O defects', and this excitation has a character of the charge-transfer transition $O \rightarrow Zr$ in the defective polyhedrons ZrO_5^{6-}. So, we have found some analogy in the origins of the UV PL and the high-energy component of the visible PL. Therefore we have good reasons to declare that the mentioned component of the visible PL is related to radiation decay of localized excitons accompanied with the charge transfer $Zr \rightarrow O$ in the imperfect ZrO_5^{6-} polyhedrons. Similar processes can appear in Zr polyhedrons associated with imperfect molecular anions $[P_2O_6 - V_O^{/}]^{2-}$. As a result, the two PL bands, V1 and V2, appear in the PL. Enhancement of the excitation intensity observed for the band C* with increasing temperature (compare curves 1 and 2 in Fig. 5) confirms this statement, since the RVS level for the $V_O^{/}$ defects is placed lower than the V_O levels and, therefore, they are activated at higher temperatures.

As for the low-energy part of the PL spectra (i.e., the PL bands V3 and V4), it is efficiently excited by low-energy photons (see curve 3 in Fig. 3 and curve 1 in Fig. 5). This fact indicates participation of the FOVS and the RVS levels in excitation of the visible PL. In other words, this PL is excited inside the A* and B* excitation bands. If the transitions take place inside the A* band, direct excitation of the full-occupied vacancies V_O (in fact, these are F centres) can be accomplished. However, it is more probable that, after direct excitation, the electron is released from the RVS level to the CB, with following migration and recombination with the hole located at the FOVS level (in fact, it is an F^+ centre). Similar processes occur in F centres formed on the basis of $V_O^{/}$ defects. The fact that the intensity of the excitation band A* increases with increasing temperature confirms our assumptions.

Finally, excitation inside the B* band causes the PL as a result of electron transition from the FOVS levels to the CB bottom. Then the free CB electrons are trapped at the RVS states and recombine with the hole at the FOVS level. This recombination is accompanied with the PL. Such interpretation explains the fact that the characteristics of the PL excited inside the excitation bands A* and B* are similar. This gives rise to the visible PL of a complex character, manifesting itself as a set of strongly overlapping bands.

Conclusions

Summarizing, we have studied experimentally the luminescence spectra of the perfect ZrP_2O_7 crystals and the same compounds containing oxygen vacancies, and have calculated theoretically their electronic structure. The analysis of these results has resulted in revealing a possible role of the oxygen vacancies in the visible PL observed in zirconium pyrophosphate. In particular, it is ascertained that the UV luminescence is accompanied with the $Zr \rightarrow O$ charge-transfer and is related to radiation decay of self-trapped excitons, where the electron component is located at the Zr^{4+} ion and the hole component is at the O^{2-} ion.

The visible luminescence has a complex character. The most probable nature of its high-energy component (2.5÷3.5 eV) is radiation decay of excitons localized at a defective Zr octahedron, ZrO_5^{6-} plus oxygen vacancy. The low-energy component of the visible PL (1.5÷2.5 eV) should be mainly caused by recombination processes, with participation of F centres formed on the basis of oxygen vacancies of the two types: one of them is the vacancy of 'bridge' oxygen, while the other is in 'non-bridge' positions.

Experimental verification of our main conclusions (in particular, the luminescence spectroscopy of ZrP_2O_7 crystals annealed in vacuum, and in reducing and oxygen atmospheres) will be the aim of our further investigations.

Acknowledgements

The authors are grateful to the researchers of scientific group headed by the Corresponding Member of the National Academy of Science of Ukraine, Professor M S Slobodyanik, for synthesis of powdered ZrP_2O_7 crystals. We also thank Senior Researcher Yu Hizhnyi for consulting on theoretical simulation procedures and Leading Engineer V Scherbatskii for his aid during experimental investigations. The studies were supported by SFFR (DFFD) of Ukraine: common Ukrainian-Belorussian Project # F54.1/0.40.

References

1. Kaneyoshi M, 2006. Luminescence of some zirconium-containing compounds under vacuum ultraviolet excitation. J. Lumin. **121**: 102–108.
2. Wu Ch and Wang Y, 2007. Study of excitation spectra of ZrP_2O_7:Tb in vacuum ultraviolet region. Mater. Lett. **61**: 5037–5039.
3. Torardi C C, Miao C R and Li J, 2003. Efficient UV-emitting X-ray phosphors: octahedral $Zr(PO_4)_6$ luminescence centers in potassium hafnium–zirconium phosphates $K_2Hf_{1-x}Zr_x(PO_4)_2$ and $KHf_{2(1-x)}Zr_{2x}(PO_4)_3$. J. Solid State Chem. **170**: 289–293.
4. Miao C R and Torardi C C, 2000. A new high-efficiency UV-emitting X-ray phosphor, $BaHf_{1-x}Zr_x(PO_4)_2$. J. Solid State Chem. **155**: 229–232.
5. Hizhnyi Yu, Chornii V, Nedilko S, Slobodyanik M, Zatovsky I, Terebilenko K and Boyko V, 2013. Luminescence spectroscopy and electronic structure of ZrP_2O_7 and $KZr_2(PO_4)_3$ crystals. http://dx.doi.org/10.1016/j.radmeas.2013.01.068.

6. Brixner L H and Blasse G, 1991. Ultraviolet luminescence from hafnium pyrophosphate (HfP_2O_7). J. Solid State Chem. **91**: 390–393.
7. Nedilko S, Nagornii P, Nedyelko I, Scherbatskii V, Stus N, Gomenyuk O, Sheludko V, Boyko V and Boyko R, 2009. Nature of intrinsic and impure luminescence of $MAlP_2O_7$ crystals. Opt. Mater. **31**: 1828–1830.
8. Smits K, Grigorjeva L, Millers D, Sarakovskis A, Grabis J and Lojkowski W, 2011. Intrinsic defect related luminescence in ZrO_2. J. Lumin. **131**: 2058–2062.
9. Petrik N G, Taylor D P and Orlando T M, 1999. Laser-stimulated luminescence of yttria-stabilized cubic zirconia crystals J. Appl. Phys. **85**: 6770–6776.
10. Zimmerer G, 2007. SUPERLUMI: A unique setup for luminescence spectroscopy with synchrotron radiation. Radiat. Meas. **42**: 859–864.
11. Blaha P, Schwarz K, Madsen G, Kvasnicka D and Luitz J, 2001. WIEN2k, An Augmented Plane Wave + Local Orbitals Program for Calculating Crystal Properties. Karlheinz Schwarz, Techn. Universität Wien, Austria. ISBN 3-9501031-1-2.
12. Huang C H, Knop O, Othen D A and Woodhams F W D, 1975. Pyrophosphates of tetravalent elements and Moessbauer study of SnP_2O_7. Can. J. Chem. **53**: 79–82.
13. Kralik B, Chang E K and Louie S G, 1998. Structural properties and quasiparticle band structure of zirconia. Phys. Rev. B. **57**: 7027–7036.
14. Spassky D A, Vasil'ev A N, Kamenskikh I A, Mikhailin V V, Savon A E, Hizhnyi Yu A, Nedilko S G and Lykov P A, 2011. Electronic structure and luminescence mechanisms in $ZnMoO_4$ crystals. J. Phys.: Condens. Matter. **23**: 365501.

Nedilko S. and Chornii V. 2013. Electronic band structure and luminescence properties of powdered ZrP_2O_7 crystals. Ukr.J.Phys.Opt. **14**: 187 – 195.

Анотація. *У роботі досліджено фотолюмінесцентні властивості кристалів ZrP_2O_7 в ультрафіолетовій і видимій ділянках спектра за умови збудження фотонами з енергією 3.5÷12 еВ. За повнопотенціальним лінеаризованим методом приєднаних плоских хвиль розраховано парціальні густини електронних станів для досконалих кристалів і кристалів, що містять два типи кисневих вакансій. УФ–люмінесценцію розглянуто як випромінювальний розпад локалізованих екситонів, сформованих на основі багатогранника $[ZrO_6]^{8-}$. Генерація екситонів в основному пов'язана з електронними переходами з переносом заряду між електронними станами Op і Zrd. Люмінесценцію у видимій ділянці спектра пов'язано з процесами, які відбуваються в багатограннику, що містить кисневі вакансії.*